7 - 12 SEPTEMBER 2014, KRAKÓW
FORUM ACUSTICUM

Hybrid Acoustic Modelling of Historic Spaces Using Blender

Jelle van Mourik
Department of Electronics, University of York, York, United Kingdom.

Stephen Oxnard
Department of Electronics, University of York, York, United Kingdom.

Aglaia Foteinou
Department of Music and Music Technology, University of Wolverhampton, Wolverhampton, United Kingdom.

Damian T. Murphy
Department of Electronics, University of York, York, United Kingdom.

Summary
Historic spaces provide a challenge in terms of achieving accurate acoustic modelling and auralisation due to the large volumes typically involved, implying significant computational overhead, uncertainty in terms of the construction materials' properties, and translating this into appropriate physically based boundary conditions. Hybrid acoustic modeling approaches seek to solve the computational problem through complementary assimilation of various modeling paradigms. SonicRender is such a hybrid acoustic modelling tool, based around the Blender open source 3D graphics development platform. Finite Difference Time Domain and ray tracing methods are used, with the FDTD method constrained to low-frequencies enabling the simulation of wave characteristics at manageable computational cost. Efficient rendering of spectrally complete RIRs are produced by combining results from geometric and band-limited numerical simulations. In this study, SonicRender is applied to recreate the acoustic of a site of historical and architectural importance: the National Centre for Early Music, York, UK. A series of acoustic measurements have been made through utilisation of the Exponential Swept Sine method for one source location and multiple receiver locations. As such, objective acoustic data is used to test the validity of SonicRender as an acoustic simulation tool through comparison of recorded and simulated room acoustic metrics. Conclusions are drawn on the future potential for using such hybrid acoustic modeling methods in similar challenging application areas.

PACS no. 43.55.Nn

1. Introduction

Computer imaging and visualisation have long been used in archaeology as a means to interpret data and test potential hypotheses as to how a particular site, landscape, building or location might have looked or been used over the its particular history. It is now perhaps becoming accepted that a better understanding and preservation of such heritage can be achieved by also considering the acoustic properties of specific sites and landscapes. Considering such acoustic characteristics therefore better enables us to develop a more complete understanding of the past, and auralisation provides the key to rendering these environments based on given data and expert interpretation of the historic or archaeological record. There exist many different methods that can be applied to the acoustic modelling and rendering of a site that no longer exists, or only exists in part, and this paper presents a hybrid method based on two existing techniques.

Two kinds of modelling algorithms are generally understood: wave-based methods, which employ a rigorous numerical solution to the wave equation, thereby able to model wave effects such as diffraction and wave interference, and geometric methods, which generally model sound as propagating along straight lines [1]. Wave-based methods are generally computationally intensive, and include methods such as the Digital Waveguide (DWG) algorithm [2, 3, 4], Finite Difference Time Domain (FDTD) method [5, 6, 7], and

Boundary Element Method [8, 9]. Particularly the FDTD method has grown in popularity over the last decade, as the algorithm is well understood, easy to implement, and the lends itself well to parallel computing implementations [7, 10]. The memory requirements grow cubically as a function of desired frequency modelled, however, which makes it unsuitable for high-frequency modelling. Geometric modelling methods on the other hand trace 'sound rays' through the acoustic space, generally starting at the source and registering an impulse when they hit the receiver. Typically, they model sound energy rather than a pressure and/or velocity field [1]. Among geometric algorithms are the Image Source Method (ISM) [11, 12], ray tracing methods [13, 14, 15], of which pyramid and cone tracing are particular implementations [16, 17], and beam tracing [18, 19]. Due to the underlying assumptions of ray-like sound propagation, these methods are not well-suited to model low frequency wave propagation, where diffraction effects are more prominent. The advantages of these methods (with exception of the image source method, which has exponential time complexity), is that they require a relatively small amount of memory and have a high performance: they can often trace thousands of paths with hundreds of reflections in a matter of seconds.

Of particular interest to this study are hybrid modelling approaches. As each method has its own relative advantages and disadvantages, a combination of multiple modelling methods has the potential to combine the best features while minimising those aspects that are non-optimal. Two commonly known hybrid acoustic modelling approaches are shown off by the commercially available acoustic modelling software ODEON [20] and CATT-Acoustic [21], which combine the ISM and, respectively, ray tracing and cone tracing. Southern *et al.* [22, 23] combined the results from an FDTD and a ray tracing algorithm into a hybrid room impulse response (RIR) of several scenes of varying complexity. Another hybrid model, showing off a (2D and 3D) DWG method in conjunction with a ray tracer, was presented by Beeson and Murphy [4].

This paper investigates the validity of a hybrid room acoustic model in a complex scene. The low end (< 355 Hz) is modelled by the FDTD algorithm whereas the middle and high parts of the spectrum are modelled using an acoustic ray tracer. These simulated IRs are then compared to their recorded counterparts. The structure of this paper is as follows: Section 2 describes the details of the FDTD and ray tracing algorithm we employed, and the post-processing steps to combine the octave bands into one IR. It also describes the recording process in which the measured IRs were obtained. Section 3 compares the recorded and simulated IRs and discusses the validity of our simulations. Conclusions and recommendations for future research are given in 4.

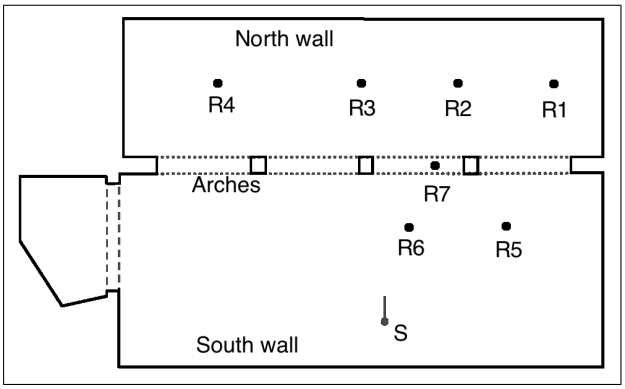

Figure 1. The source (S) and receiver (R1–R7) positions on the floor plan of the National Centre for Early Music.

2. Methods

The studied space was St. Margaret's Church in York, United Kingdom, currently known as the National Centre for Early Music. The church has been acoustically treated for concerts and conference use, with reversible acoustic panels and drapes arranged throughout the space to easily change the physical acoustic characteristics [24]. For the purpose of this study, the acoustic configuration referred to as 'musical/opera performances' was used. For this configuration drapes and 75% of the panels were in use (open). The remaining folded panels were the ones on the north wall. During the impulse response measurements in the actual space, the temperature was measured at a constant 21.5°C and the relative humidity at 44.5-45%. The space was empty, without any audience or seating. The main space contained several pieces of furniture, such as a piano, several tables, and a harpsichord.

2.1. Recorded impulse responses

Impulse response measurements in the church were made using the Exponential Swept Sine (ESS) Method [25], with the Aurora plug-in [26] for analysis of the acoustical parameters. The frequency range of the sine sweep was from 22Hz to 22kHz, and lasted 15 seconds, using a Genelec S30D as the source transducer, and a Soundfield SPS422B as the receiver microphone. The source was placed as a performer would be in the space, facing towards the north wall, while the microphone was aligned toward the south wall for each location. Although during the measurements process 26 receiver positions were used for an appropriate acoustic coverage of the space, seven receiver positions are used in this research. These receivers are selected according to the nature of their position so as to give a representative sample of the room. Fig. 1 shows a floor plan of the space, with source (S) and receivers (R1–R7) marked.

Table I. The absorption coefficients used in the NCEM model.

Material	Absorption coefficients {62.5Hz, 125Hz, 250Hz, 500Hz, 1kHz, kHz, 4kHz, 8kHz}
Main wall	{ 0.02, 0.02, 0.02, 0.03, 0.04, 0.05, 0.05, 0.05 }
Main floor	{ 0.01, 0.01, 0.02, 0.03, 0.07, 0.09, 0.10, 0.10 }
Wood	{ 0.10, 0.10, 0.07, 0.05, 0.04, 0.04, 0.10, 0.10 }
Stone	{ 0.04, 0.05, 0.06, 0.06, 0.05, 0.05, 0.06, 0.05 }
Windows	{ 0.10, 0.10, 0.07, 0.05, 0.05, 0.02, 0.02, 0.02 }
Plastic	{ 0.10, 0.10, 0.25, 0.45, 0.58, 0.65, 0.70, 0.70 }
Reflectors	{ 0.001, 0.15, 0.05, 0.05, 0.04, 0.05, 0.14, 0.14 }
Marble	{ 0.001, 0.01, 0.01, 0.01, 0.01, 0.02, 0.02, 0.02 }
Fabric	{ 0.03, 0.03, 0.04, 0.11, 0.17, 0.24, 0.35, 0.35 }
Drapes	{ 0.14, 0.14, 0.35, 0.55, 0.72, 0.70, 0.65, 0.65 }

2.2. Simulated impulse responses

The aim of this research was to obtain high-accuracy IRs of the above described space using our modelling software. To this end, we endeavored to model the space as accurately as possible. The following sections describe the design stage and the algorithms we employed for the room acoustic simulations.

2.2.1. Blender design stage

The design stage was done using the open source 3D modelling software Blender 2.69 [27]. Using Blender's user interface allows for a quick creation of the geometry and material assignment of the scene. A plugin for this programme, first introduced in [28], was used to add acoustical data to the materials of each surface in octave bands from 62.5 Hz to 8 kHz. The plugin exports the geometry and material data to an intermediate Wavefront (.obj) geometry file, which is subsequently read by the ray tracer and FDTD solver.

Information regarding the acoustic characteristics of the surfaces, absorption and scattering coefficients, was gathered from existing libraries and literature of previous modeling work, such as [29, 30, 31, 32], and the most appropriate values were chosen for each surface in the space. Table I shows the materials we used and their absorption coefficients across the eight frequency bands.

2.2.2. FDTD simulation

The lower three octave bands (mid-frequencies: $\{62.5\text{ Hz}, 125\text{ Hz}, 250\text{ Hz}\}$) have been simulated using a second-order FDTD scheme [33, 34]. This commonly used discrete-time approximation method, though computationally intensive, is a good way to model wave-based effects such as diffraction and wave interference. The internal domain of the acoustic space was voxelised into a rectilinear grid and divided into 1) material nodes: nodes that represent a solid material and do not have a pressure value associated with them, and hence do not need to be updated, 2) boundary node: nodes that border at least one material node, and 3) air nodes, which border only boundary and/or other air nodes. The homogeneous wave equation is a good model for the propagation of sound:

$$\frac{\partial^2}{\partial t^2} p(\mathbf{x}, t) = c^2 \nabla^2 p(\mathbf{x}, t)\,, \tag{1}$$

where $p(\mathbf{x}, t)$ represents the sound pressure as a function of position $\mathbf{x}$ and time t. The speed of sound c in our model is $343.26\frac{m}{s}$, and the spatial second derivative in Cartesian coordinates is $\nabla^2 = \frac{\partial^2}{\partial x^2} + \frac{\partial^2}{\partial y^2} + \frac{\partial^2}{\partial z^2}$. For 3-dimensional pressure values in discrete time, we use the short-hand notation $p^t_{i,j,k} \triangleq p(xX, yX, zX, tT)$, where x, y, z represent the position in 3D space, X is the grid spacing, and T is the time step.

The Standard Rectilinear (SRL) stencil was used to update the air nodes. This stencil is derived using a second-order difference approximation across each axis to arrive at the update equation:

$$p^{t+1}_{i,j,k} = (2 - 6\lambda^2) p^t_{i,j,k} - p^{t-1}_{i,j,k} + \lambda^2 \sum_{f \in \text{faces}} p^t_f, \tag{2}$$

where p^t_f, represent the six neighboring faces of the air node and $\lambda = \frac{cT}{X}$ is the Courant number, chosen at its stability limit $\frac{1}{\sqrt{3}}$. In our model, the spatial step X was 7.5 cm, such that the sample rate $f_s = \frac{1}{T}$ of the model was 7927 Hz.

The boundary node's update equation depends on the impedance value of the neighbouring material(s). At a boundary, the following impedance relationship holds for waves at normal incidence:

$$\frac{\partial}{\partial t} p(\mathbf{x}, t) = -\zeta\, \nabla p(\mathbf{x}, t), \tag{3}$$

where ζ is the relative impedance value of the material (see e.g. [35, p.32]). As the grid is rectilinear, incidence at a grazing angle doesn't need to be considered. The conversion from absorption value α to impedance value is as follows:

$$\frac{1 + \sqrt{1 - \alpha}}{1 - \sqrt{1 - \alpha}}, \tag{4}$$

for a phase-preserving boundary [36]. If we discretise Eq. 4 by approximating the time derivative with a centred and the spatial derivative with a forward difference operator, we can substitute the result into Eq. 2 to obtain the results derived in [10]. This can easily be extended to work for boundary nodes neighbouring multiple materials of potentially different impedance values.

2.2.3. Ray tracer

The ray tracing algorithm finds its roots in the field of graphics [37, 38], and has since made its way to the field of acoustics. It inherently assumes ray-like behaviour, which is only a valid approximation for high frequencies. At low frequencies, diffraction and standing wave effects are more prominent, such that a ray tracer does not produce reliable results. Therefore, only the upper 5 octave bands $\{500\text{ Hz}, 1\text{ kHz}, 2\text{ kHz}, 4\text{ kHz}, 8\text{ kHz}\}$) were modelled by our ray tracer.

The ray tracing method we employ is forward ray tracing, i.e. tracing rays from the source to the listeners. Though backward ray tracing has advantages particularly in real-time acoustic ray tracing [39] , forward ray tracing is more optimal in our case, as it can exploit the fact that we have one sound source and multiple listeners.

The omnidirectional source was modelled by casting 10^7 rays in pseudo-random directions by sampling a unit sphere. The high number of rays provides for a representative sample of the unit sphere. Every material in the scene has a Bidirectional Reflectance Distribution Function (BRDF) $f(\boldsymbol{\omega}_i, \boldsymbol{\omega}_o)$ associated with it [40]. For a given incoming and outgoing angle $\boldsymbol{\omega}_i$ and $\boldsymbol{\omega}_o$ with respect to the surface normal, $f(\boldsymbol{\omega}_i, \boldsymbol{\omega}_o)$ is the reflected sound energy. It is bidirectional, which means that $f(\boldsymbol{\omega}_i, \boldsymbol{\omega}_o) = f(\boldsymbol{\omega}_o, \boldsymbol{\omega}_i)$. The rendering equation [41] states that the outgoing ray energy $L_o(\mathbf{x}, \boldsymbol{\omega}_o, t)$ can be expressed in the following terms:

$$L_o(\mathbf{x}, \boldsymbol{\omega}_o, t) = L_e(\mathbf{x}, \boldsymbol{\omega}_o, t) + \ldots \int f(\mathbf{x}, \boldsymbol{\omega}_i, \boldsymbol{\omega}_o)\, L_i(\mathbf{x}, \boldsymbol{\omega}_i, t) \cos\theta_i \, d\boldsymbol{\omega}_i \,, \quad (5)$$

where $L_e(\mathbf{x}, \boldsymbol{\omega}_o, t)$ is the emitted sound energy and $L_i(\mathbf{x}, \boldsymbol{\omega}_i, t)$ is the incoming sound energy under angle $\boldsymbol{\omega}_i$ at time t. As the emitted sound is 0 everywhere except for at the sound source, this term can be ignored and the sound source can be treated as a special case.

The BRDF we employ is loosely based around the Phong scattering model [42]. This is a simplified model of a scatterer that allows for defining a scattering function that is anything between a specular reflector and a Lambertian reflector, based on the exponent factor k.The formal description of the BRDF of the Phong scatterer is:

$$f_{\text{Phong}}(\boldsymbol{\omega}_i, \boldsymbol{\omega}_o) = (1-\alpha)\frac{k+1}{2\pi}\cos^k\left(\boldsymbol{\omega}_o \cdot \boldsymbol{\omega}_{\text{spec}}\right), \quad (6)$$

where k is some factor relating to the diffusion coefficient μ, and $\boldsymbol{\omega}_{\text{spec}}$ is the specular reflection of $\boldsymbol{\omega}_i$. Fig. 2 shows the scattering distribution for different values of k. When $k = 1$, the surface behaves as a Lambertian reflector. For high values of k, it behaves in a predominantly specular fashion.

The sound receiver we used was a point receiver. Instead of registering physical ray hits as is common for a spherical receiver, the point receiver registers an impulse based on the reflected sound energy at each reflection, which can be computed exactly using Eq. 6. The advantage of this is that the contribution of a large number of (often small) hits can be registered), with no potential error related to the size or shape of the receiver chosen. Air absorption for each octave band was modelled using the air absorption coefficient at mid-frequency of each octave band. The air absorption coefficients were computed using the formula by Bass *et al.* [43] using the atmospheric conditions as described earlier in this section.

Table II. Overview of cut-off frequencies applied in the octave band filter bank.

Octave Band (Hz)	Lower Cut-off (Hz)	Upper Cut-off (Hz)
62.5	0	82
125	82	177
250	177	355
500	355	710
1000	710	1420
2000	1420	2840
4000	2840	5680
8000	5680	11360

2.3. Combining octave bands

As the simulated IRs are computed separately for each frequency band, they need to be combined appropriately into a single RIR. To this end, a simple octave band approach was utilised (see e.g. [44]). This method combines the valid pass band, defined by the frequency range over which the absorption coefficients are applicable, of each impulse response by first band-pass filtering the responses around suitable cut-off frequency values and then summing the resulting signals. In this work, a bank of first order Butterworth filters was utilised, giving a 3 dB/octave reduction in magnitude above and below the defined cut-off frequencies provided in Table II. After the band-pass filtering, the FDTD and ray-traced IRs were summed to produce the total IR.

As the FDTD and ray traced IRs are computed separately, they need to be combined in such a way that their respective energy levels are calibrated correctly. A number of energy calibration algorithms are described in related literature, e.g. [22, 45, 23]. For the purposes of this work, a simple energy calibration procedure, as discussed in [22], was deemed most suitable. More rigorous calibration techniques, such as described in [23], are valid only for high resolution FDTD schemes with temporal sampling frequencies greater than 18kHz, which was not feasible in this

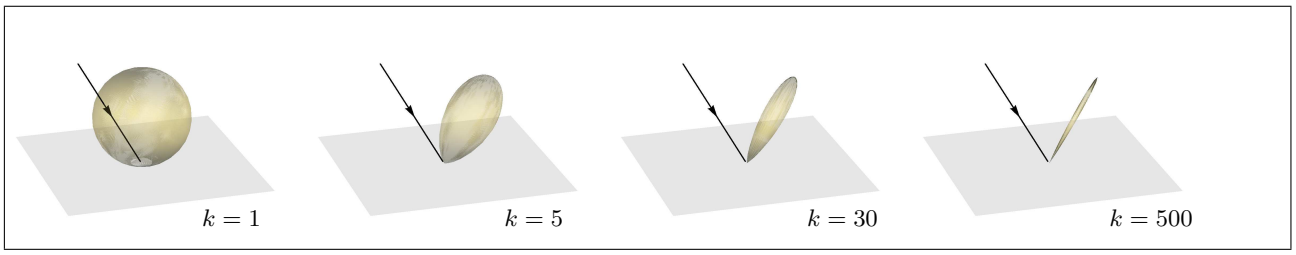

Figure 2. Phong scattering lobes with different coefficients for k.

study. Following [22], a calibration parameter can be expressed as:

$$\eta = \frac{(f_2 - f_1)\sum_{i=g_1}^{g_2} |G_{IR}[i]|}{(g_2 - g_1)\sum_{i=f_1}^{f_2} |N_{IR}[i]|} \tag{7}$$

The above expression calculates the ratio of average magnitudes in the frequency spectrum of the high frequency ray-tracer IRs, G_{IR}, and low frequency FDTD IRs, N_{IR}, over a finite series of discrete frequency ranges $[f_1; f_2]$ and $[g_1; g_2]$ with index i. The FDTD IRs were calibrated with f_2 and g_1 set equal to the crossover frequency between low and high frequency IRs: $f_2 = g_1 = 355$ Hz. The upper and lower bounds of the frequency ranges were defined as $f_1 = 100$ Hz and $g_2 = 610$ Hz, hence the ratio of average magnitudes over a range of 255Hz above and below the crossover frequency was calculated and applied to each FDTD IR by multiplication for each IR.

Although this energy matching procedure is prone to several types of errors [22], it was deemed sufficient for the purposes of informal listening tests and octave band RIR analysis. Having calibrated the low frequency portion of each IR, the total IRs were created by summing the calibrated signals to the corresponding high frequency portions.

3. Results

The acoustic parameters used for comparison were T_{30} and Early Decay Time (EDT). Other parameters, such as Clarity and Definition, were deemed inappropriate for comparison, as the simulation did not take into account the source directivity of the sound source. It was shown by Fouteinou [46, p. 64, p. 137] that the directionality of the source can have a great impact on the values of these parameters, and thus a comparison would not be directly meaningful.

The results of the T_{30} times are presented in Fig. 3. The measurement data, simulation data, and their difference are plotted alongside each other. The measurements and the simulations show a similar behaviour, though there are significant differences in the first three octave bands. The overall mean difference between measurement and simulation is 0.11 seconds, with a standard deviation of 0.13 s. The largest error is found in the 62.5 Hz octave band, which has a consistently too high estimation of T_{30}. The octave bands 125 Hz and 250 Hz are on the whole estimated too low. This causes a clearly visible dip in the decay time around these frequencies. The reverberation time at the 8 kHz band is consistently too high in the simulations, compared to the measurements.

There are several possible explanations for the deviations in T_{30}. On the one hand, the absorption values in the model may not be accurate enough. Moreover, low values produced by the FDTD algorithm can also be explained by the fact that the surface area in the voxelised space is always overrepresented, whereas the volume is underrepresented. From the Eyring equation it follows that this will lead to a lower reverberation. This however does now explain why the 62.5 Hz band shows a significantly too high T_{30}. The lack of a steep roll-off in the 8 kHz band could be partially explained by the fact that the air absorption coefficient used is based on a mid-frequency value. Using a weighted absorption coefficient over the entire octave band would result in higher absorption, and thus a steeper roll-off.

Fig. 4 shows the analysis results of the EDT values. On the whole, they vary a lot more across receivers than the T_{30} results, which is expected behaviour. It appears that the simulated IRs do not simulate these differences accurately, however: the mean difference between the EDT values of the measured and simulated IRs across all frequencies is 0.18 s, with a standard deviation of 0.24 s. In contrast to the T_{30} values, there is no clear trend in the way the simulated IRs deviate from their measured counterparts, though the FDTD bands seem to produce larger errors than the ray traced ones. EDT is much more susceptible to changes in early reflections, and so a more in depth analysis and comparison between modelled and measured first reflection patterns should be considered as part of further work.

4. Conclusion

In this study, we demonstrated the use of the hybrid acoustic modelling software SonicRender for modelling a relatively large historic space. We show that the design stage of the acoustical model can be greatly enhanced using dedicated 3D design software such as Blender. We present a hybrid acoustic model that uses

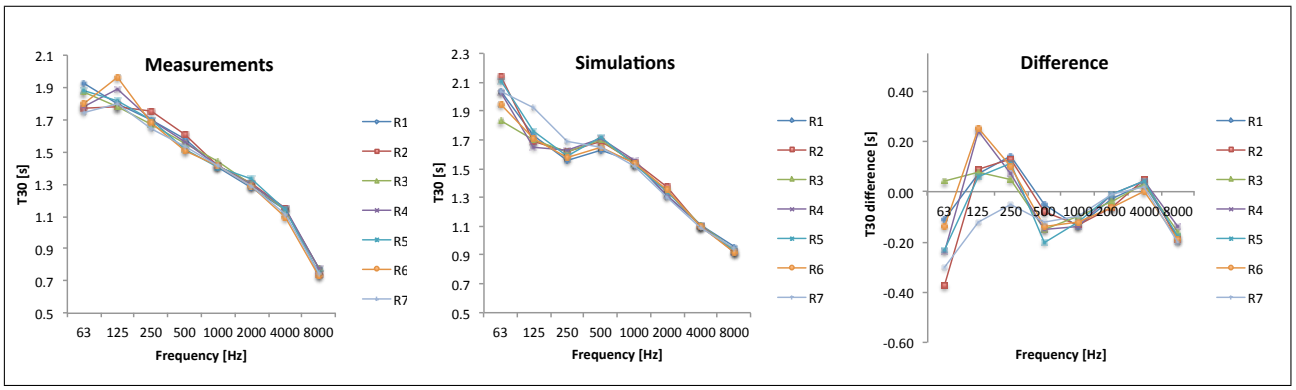

Figure 3. The T_{30} values for the measured IRs, simulated IRs, and the difference between the two, across all frequency bands.

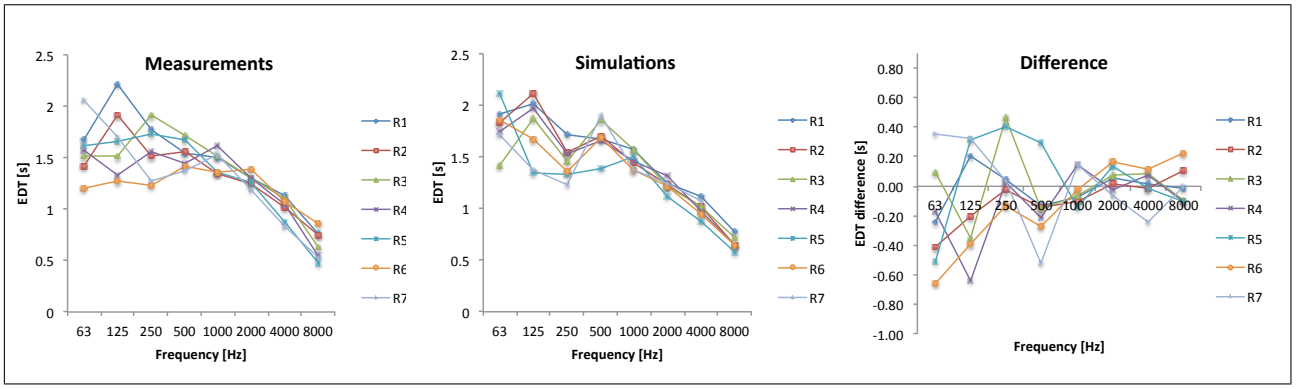

Figure 4. The EDT values for the measured IRs, simulated IRs, and the difference between the two, across all frequency bands.

FDTD modelling for the three lowest octave bands and our own ray tracing algorithm for the high frequency models. Though the results for the T_{30} time are stable across the space—which points in favour of our approach—the values only moderately correspond to those of the recorded IRs. There are several possible reasons for this, and it is impossible to say if this is due to incorrect data at the design stage or due to shortcomings in the algorithms. The EDT values of the recordings vary a lot for the different receivers, more so at low frequencies. At high frequencies, these values are estimated fairly correctly, but at low frequencies our model fails to reproduce similar values. Other acoustic parameters have not been examined, as source directivity isn't currently modelled by our hybrid model, though this has a significant effect on the results.

Formal comparisons between measured and simulated IRs are an essential part of validating acoustic simulation methods. Future research will focus on different, potentially less complex spaces in order to obtain reliable conclusions of the validity of the model. Incorporating source directivity is an essential part of this, as nearly all physical sound sources have non-uniform directivity pattern, especially at high frequencies. Formal listening tests would be a valuable source of information on the perceived quality of the modelled IRs and on the noticeable differences for different receiver locations in the same space.

Acknowledgement

The authors would like to thank the National Centre for Early Music, York, for access to their site and development plans. This work is supported in part by the Department of Electronics at the University of York

References

[1] S. Siltanen, T. Lokki, and L. Savioja, "Rays or waves? Understanding the strengths and weaknesses of computational room acoustics modeling techniques," in *Proceedings of the International Symposium on Room Acoustics 2010*, pp. 1–6, August 2010.

[2] J. O. Smith, "Physical modeling using digital waveguides," *Computer Music Journal*, vol. 16, no. 4, pp. 74–91, 1992.

[3] C. Erkut and M. Karjalainen, "Finite difference method vs. digital waveguide method in string instrument modeling and synthesis," in *Proceedings of the International Symposium on Musical Acoustics*, 2002.

[4] M. J. Beeson and D. T. Murphy, "RoomWeaver: a digital waveguide mesh based room acoustics research

tool," in *Proceedings of the 7th International Conference on Digital Audio Effects (DAFX-04)*, October 2004.

[5] D. Botteldooren, "Finite-difference time-domain simulation of low-frequency room acoustic problems," *Journal of the Acoustical Society of America*, vol. 98, no. 6, pp. 3302–3308, 1995.

[6] M. van Walstijn and K. Kowalczyk, "On the numerical solution of the 2D wave equation with compact FDTD schemes," in *Proceedings of the 11th International Conference on Digital Audio Effects (DAFX-08)*, September 2008.

[7] L. Savioja, "Real-time 3D finite-difference time-domain simulation of low- and mid-frequency room acoustics," in *Proceedings of the 13th International Conference on Digital Audio Effects (DAFx-10)*, 2010.

[8] S. Kirkup, *The boundary element method in acoustics: a development in Fortran*. Integral equation methods in engineering, Integrated Sound Software, 1998.

[9] R. P. Shaw, "Diffraction of acoustic pulses by obstacles of arbitrary shape with a robin boundary condition," *Journal of the Acoustical Society of America*, vol. 41, no. 4, pp. 855–859, 1967.

[10] C. J. Webb and S. Bilbao, "Computing room acoustics with CUDA - 3D FDTD schemes with boundary losses and viscosity," in *IEEE International Conference on Acoustics, Speech and Signal Processing*, pp. 317–320, 2011.

[11] J. Borish, "Extension of the image model to arbitrary polyhedra," *Journal of the Acoustical Society of America*, vol. 75, no. 6, pp. 1827–1836, 1984.

[12] U. Kristiansen, A. Krokstad, and T. Follestad, "Extending the image method to higher-order reflections," *Applied Acoustics*, vol. 38, no. 2–4, pp. 195–206, 1993.

[13] H. Lehnert, "Systematic errors of the ray-tracing algorithm," *Applied Acoustics*, vol. 38, no. 2–4, pp. 207–221, 1993.

[14] M. Vorländer, "Simulation of the transient and steady-state sound propagation in rooms using a new combined ray-tracing/image-source algorithm," *Journal of the Acoustical Society of America*, vol. 86, pp. 172–178, 1989.

[15] A. M. Ondet and J. L. Barbry, "Model of sound propagation in fitted workshops using ray tracing," *Journal of the Acoustical Society of America*, vol. 85, no. 2, pp. 787–796, 1989.

[16] A. Farina, "Validation of the pyramid tracing algorithm for sound propagation outdoors: comparison with experimental measurements and with the iso-dis 9613 standards," *Advances in Engineering Software*, vol. 31, no. 4, pp. 241 – 250, 2000.

[17] B.-I. Dalenbäck, "Verification of prediction based on randomized tail-corrected cone-tracing and array modeling," in *137th Convention of the Acoustical Society of America*, 1999.

[18] I. A. Drumm and Y. W. Lam, "The adaptive beam-tracing algorithm," *Journal of the Acoustical Society of America*, vol. 107, no. 3, pp. 1405–1412, 2000.

[19] T. Funkhouser, N. Tsingos, I. Carlbom, G. Elko, M. Sondhi, J. E. West, G. Pingali, P. Min, and A. Ngan, "A beam tracing method for interactive architectural acoustics," *Journal of the Acoustical Society of America*, vol. 115, pp. 739–756, Feb. 2004.

[20] Odeon, "Odeon | Room Acoustics | Noise Prediction Software." Online source: `http://www.odeon.dk/`. Last accessed: May 27, 2014.

[21] CATT-Acoustic, "CATT-Acoustic | The FIReverb Suite | ReflPhinder." Online source: `http://www.catt.se`. Last accessed: May 27, 2014.

[22] A. P. Southern, S. Siltanen, and L. Savioja, "Spatial room impulse responses with a hybrid modeling method," in *Proceedings of the 130th Audio Engineering Society Convention*, 2011.

[23] A. P. Southern, S. Siltanen, D. T. Murphy, and L. Savioja, "Room impulse response synthesis and validation using a hybrid acoustic model," *IEEE Transactions on Audio, Speech, and Language Processing*, vol. 21, no. 9, pp. 1940–1952, 2013.

[24] National Centre For Early Music, "NCEM History." Online source: `http://www.ncem.co.uk/`, 2014. Last accessed: May 27, 2014.

[25] A. Farina, "Simultaneous measurement of impulse response and distortion with a swept-sine technique," *Proceedings of the 108th AES Convention*, 2000.

[26] A. Farina, "Aurora plug-ins." Online source: `http://www.aurora-plugins.com/`, 2007. Last accessed: May 27, 2014.

[27] Blender Foundation, "Blender 2.69." [Computer programme] Retrieved from: `www.blender.org`, 2014. Last accessed: May 24, 2014.

[28] J. van Mourik and D. T. Murphy, "Geometric and wave-based acoustic modelling using Blender," in *Proceedings of the AES 49th International Conference, Audio for Games*, 2013.

[29] I. Bork, "A comparison of room simulation software - the 2nd round robin on room acoustical computer simulation," *Acta Acustica*, vol. 86, pp. 943–956, 2000.

[30] M. Lisa, J. H. Rindel, and C. L. Christensen, "Predicting the acoustics of ancient open-air theaters: The importance of calculation methods and geometrical details," in *Joint Baltic-Nordic Acoustics Meeting*, 2004.

[31] A. L. Álvarez, T. A. Z. no, S. T. Giròn, and M. S. Galindo, "Virtual acoustics of the cathedral of Malaga (Spain)," in *Proceedings of Forum Acusticum 2011*, 2011.

[32] U. Berardi, "Simulation of acoustical parameters in rectangular churches," in *Journal of Building Performance Simulation*, vol. 6, 2013.

[33] D. Botteldooren, "Acoustical finite-difference time-domain simulation in a quasi-Cartesian grid," *Journal of the Acoustical Society of America*, vol. 95, no. 5, pp. 2313–2319, 1994.

[34] L. Savioja, T. J. Rinne, and T. Takala, "Simulation of room acoustics with a 3-D finite difference mesh," in *Proceedings of the International Computer Music Conference*, pp. 463–466, 1994.

[35] D. Blackstock, *Fundamentals of physical acoustics*. Wiley-Interscience, John Wiley & Sons, 2000.

[36] L. E. Kinsler, A. E. Frey, A. B. Coppens, and J. V. Sanders, *Fundamentals of Room Acoustics*. John Wiley & Sons, Fourth ed., 2000.

[37] A. Appel, "Some techniques for shading machine renderings of solids," in *Proceedings of the AFIPS Spring Joint Computer Conference*, pp. 37–45, 1968.

[38] T. Whitted, "An Improved Illumination Model for Shaded Display," in *Graphics and Image Processing* (J. D. Foley, ed.), vol. 23, pp. 343–349, Bell Laboratories, 1980.

[39] C. Schissler and D. Manocha, "GSound: Interactive sound propagation for games," in *Proceedings of the 41st AES Conference: Audio for Games*, 2011.

[40] F. E. Nicodemus, "Directional reflectance and emissivity of an opaque surface," *Applied Optics*, vol. 4, no. 7, pp. 767–775, 1965.

[41] J. T. Kajiya, "The rendering equation," *SIGGRAPH Computer Graphics*, vol. 20, pp. 143–150, August 1986.

[42] B. T. Phong, "Illumination for computer generated pictures," *Communications of the Association for Computing Machinery*, vol. 18, no. 6, pp. 311–317, 1975.

[43] H. E. Bass, L. C. Sutherland, and A. J. Zuckerwar, "Atmospheric absorption of sound: Update," *The Journal of the Acoustical Society of America*, vol. 88, no. 4, pp. 2019–2021, 1990.

[44] J. D. Schäffer, B. M. Fazenda, J. A. S. Angus, and D. T. Murphy, "A simple multiband approach for solving frequency dependent problems in numerical time domain methods," in *Proceedings of Forum Acusticum 2011*, pp. 269–274, 2011.

[45] S. Siltanen, A. P. Southern, and L. Savioja, "Finite-difference time domain method source calibration for hybrid acoustics modeling," in *IEEE International Conference on Acoustics, Speech and Signal Processing*, pp. 166–170, 2013.

[46] A. Foteinou, *Perception of Objective Parameter Variations in Virtual Acoustic Spaces*. PhD thesis, University of York, 2013.